Detection of Influential Nodes in Network Dynamical Systems from Time-Series

Pietro De Lellis[1⋆] and Maurizio Porfiri[2,3⋆]

***Abstract*—Identifying influential nodes in network dynamical systems requires the manipulation of tolopogical and dynamic characteristics within ideal experiments. However, seldom do we have access to experimental settings that could afford targeted interventions or to calibrated mathematical models that could support faithful what/if analyses. Our knowledge of the network dynamical system is often limited to the time-series of individual nodes in some real experiment. Using these time-series, it is possible to undertake a number of inference tasks, from reconstructing the topology of the network to discovering hidden nodes. Whether or not time-series of real experiments could help pinpoint causal influence within the network is an open question. Here, we address this question in the context of synchronization problems, where the influence of a node is defined as the extent to which adding noise at that particular node affects the overall synchronization of the entire network. For linear time-invariant dynamics and undirected topologies, we demonstrate the possibility of exactly detecting the most influential nodes in the network without a calibrated mathematical model, using only time-series of a real experiment where all nodes are plagued by noise. Beyond illustrating our results on classical and second-order consensus protocols, we consider two real-world datasets: firearm prevalence in the U.S. and players' movements in a soccer game. Just as our conclusions support the emergence of influential States which have a less stringent legal environment, they hint at the instrumental role of players who are critical to the offense strategy of the team.**

***Index Terms*—Consensus, synchronization, stochastic systems, vulnerability.**

I. INTRODUCTION

Social networks [1], animal groups [2], power grids [3], brain structural and functional systems [4], and climate networks [5] are all instances of network dynamical systems, where the interaction within an ensemble of coupled units could promote the emergence of collective behavior. Through the lens of network dynamical systems, researchers have studied a wide range of phenomena that are ubiquitous in science and technology. For example, several studies have investigated diffusion problems over networks, shedding light on the conditions that will beget localized versus cascading dynamics [6], [7]. Likewise, extensive efforts have been placed toward the analysis of complete or partial synchronization [8], where the network dynamical system will evolve along one synchronous manifold or multiple, coexisting manifolds.

⋆Corresponding authors: pietro.delellis@unina.it, mporfiri@nyu.edu

[1]Department of Information Technology and Electrical Engineering, University of Naples Federico II, 80125, Naples, Italy.

[2]Department of Mechanical and Aerospace Engineering, New York University Tandon School of Engineering, Brooklyn NY, US.

[3]Department of Quantitative Methods, Law and Modern Languages, Technical University of Cartagena, 30201, Cartagena, Murcia, Spain.

A fundamental question in the study of network dynamical systems pertains to the quantification of the role of each of its units on the response of the entire system. For example, in the context of power grids, it is of critical importance to identify the nodes from which a targeted attack could trigger the failure of the entire network [9]. Likewise, an open question in neuroscience entails the prediction of the effect of specific brain lesions on clinical outcomes [4]. The scientific interest toward an objective assessment of the role of specific nodes on the network dynamics extends beyond the analysis of targeted attacks, touching on a wide range of control problems [10]. From the study of pinning control in technological networks to leadership in animal groups [11], there is growing interest toward the identification of the nodes in the network from which it could be possible to effectively steer the dynamics of the entire system. In general, all these problems relate to the notion of causal influence, which, as specifically acknowledged by Lizier and Prokopenko, 'refers to the extent to which the source variable has a direct influence or drive on the next state of a destination variable, i.e. "if I change the state of the source, to what extent does that alter the state of the destination?" [12].'

The traits of influential nodes are far from trivial. Recent research has brought to light a complex interplay between dynamics and topology through numerical and analytical studies on a wide array of network dynamical systems. In addition to examining vulnerability of power grids [13]–[15] and general chaotic systems [16], [17], recent efforts have focused on leadership and optimal collective response to disturbances in consensus problems over networks [18], [19] and, more generally, networks of networks [20]. Overall, findings from these studies point at a number of counter-intuitive results, which a mere topological analysis of influence might not be able to uncover, despite its level of sophistication [21].

For example, studies on vulnerability of network dynamical systems suggest that peripheral nodes could have a key role on the overall network dynamics in power grids, but might play a secondary role in consensus protocols. Specifically, Tyloo *et al.* [13] demonstrated an inverse correlation between the nodes' resistance centrality and their influence on the transient stability of the European power grid. The more the node was peripheral, the more an applied disturbance would be effective in eliciting large excursion from synchronous power generation. On the contrary, for a class of consensus problems, applying a similar perturbation was found to have an opposite effect [17]. The network was found to be more vulnerable to targeted attacks at central nodes, which caused large steady-state variations among the nodes.

Let alone the choice of the specific performance metric

for the network dynamical system, which could vary from transient [13] to steady-state [17] features, studying causal influence requires a series of ideal experiments where the researcher can evaluate how specific manipulations at the node-level translate into network-level performance. These ideal experiments are typically based on an available mathematical model that captures the interactions between the units and their individual dynamics. However, seldom, do we have complete knowledge about the network dynamical system, whereby neither the dynamics of each individual unit nor the topology of the interconnecting network are exactly known to the researcher. In principle, a potential way around the lack of a predictive mathematical model is to experimentally probe the system through targeted interventions, but that would require fine control over experimental variables that is often unfeasible. Is it possible to identify key players in the network from real experimental observations, without either a calibrated mathematical model or the possibility to perform tailored experiments to support any manipulation of the dynamics and topology?

A tenable answer to this question can be obtained by undertaking the reconstruction of the entire network topology and the dynamics of its individual nodes. From knowledge of all the links and individual dynamics, we could construct a faithful mathematical model whose analysis will beget insight into the structure of the network, from which to embark on the identification of key players. The typical line of approach to address these issues is to formulate hypotheses on the network topology or on the individual dynamics and then pursue model identification. For example, [22] proposed a methodology to identify the dynamics of the units upon knowledge about the underlying topology; [23], [24] demonstrated the possibility of inferring the network dynamical system from the input-output transfer function; [25], [26], and [27] established effective identification procedures based on time-series for networks described by a tree and consensus-like protocols, respectively; and [28] formulated criteria and hypotheses for solving the identification problem that were the starting point for [29] to introduce an ARMAX model for heterogeneous data that involve multiple replicates.

Here, we present an alternative approach to detect key players, without the need of identifying topology and individual dynamics. Our approach does not promise insight into the network dynamical system, but, at the same time, it requires minimal hypotheses on the network topology and individual dynamics, that is, we require undirected, potentially weighted, topologies and linear dynamics. We focus on network synchronization, for which we successfully pinpoint influential nodes from time-series of real experimental observations where each node is plagued by noise, without a calibrated mathematical model or targeted experimental manipulations.

In the context of synchronization, the influence of a node is defined as the extent to which adding noise at that particular node affects the overall synchronization of the entire network, that is, the vulnerability of the network to a targeted disturbance. For a wide class of mathematical models of network synchronization, we establish a closed-form expression for the vulnerability, in terms of topological and dynamic features of the network system. In agreement with one's expectation, a disturbance added to any of the nodes affects the dynamics of all the other nodes in the network. However, the extent of this interaction can be retrieved from real experimental observations, in which noise is acting on all nodes of the network, thereby affording the inference of causal influence without either a calibrated model or tailored experimental manipulations. Such a claim is anchored in the discovery of a reciprocity principle for network dynamical systems, which extends to this field of investigation a classical tool in mechanics and electromagnetics [30], [31].

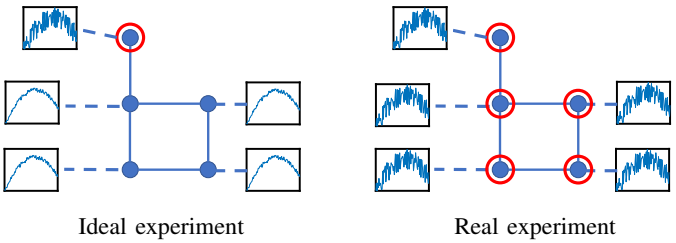

Fig. 1. The notion of causal influence is based on a sequence of ideal experiments, in which the researcher introduces a desired perturbation at a selected unit (circled in red), and observes its effect on the overall dynamics of the system from the time-series of each unit (shown as a box). In practice, these ideal experiments are not feasible and the researcher should infer causal influence from real experimental observations where noise plagues each node.

The rest of the paper is organized as follows. In Section II, we present the class of synchronization problems for which our inference approach is applicable. In Section III, we study the noisy dynamics of the network system and introduce our notion of causal influence, establishing a closed-form expression for the vulnerability of the system to noise injected at a specific node. In Section IV, we prove our main claim regarding the inference of causal influence from raw time-series. In Section V, we illustrate the validity of our approach on scalar and second-order dynamics. In Section VI, we examine two real-world applications: firearm prevalence in the United States of America and players' coordination in a soccer match. Finally, Section VII summarizes the main conclusions of the study and identifies directions for further research.

II. Dynamics of the network dynamical system

We consider a network of N identical, diffusively coupled, linear dynamical systems in a discrete-time setting. The dynamics of the i-th unit can be written as

$$x^i_{k+1} = Fx^i_k - \sum_{j=1}^{N} l_{ij}\Gamma x^j_k + q_i B\eta^i_k, \tag{1}$$

where $x^i_k \in \mathbb{R}^n$ is the state of the i-the unit at time k; $F \in \mathbb{R}^{n\times n}$ is a matrix that specifies the individual dynamics; l_{ij} is the ij-th element of the Laplacian matrix of the network $L \in \mathbb{R}^{N\times N}$, which completely encodes the network topology [32]; $\Gamma \in \mathbb{R}^{n\times n}$ is the inner coupling matrix constraining the interaction between neighboring nodes; $\eta^1_k, \ldots, \eta^N_k \in \mathbb{R}^m$ are independent identically distributed noise with zero mean and covariance matrix Σ_η; q_i is a positive scalar modulating the intensity of the noise acting on node i, with $q_i = 0$ implying that node i is not affected by noise;

Using Kronecker algebra [33], (1) can be rewritten in compact matrix form as

$$x_{k+1} = (I_N \otimes F - L \otimes \Gamma)x_k + (Q \otimes B)\eta_k, \tag{2}$$

where I_N is the identity matrix in $\mathbb{R}^N$, $x_k = \left[(x_k^1)^{\mathrm{T}}, \dots, (x_k^N)^{\mathrm{T}}\right]^{\mathrm{T}}$, $\eta_k = \left[(\eta_k^1)^{\mathrm{T}} \dots, (\eta_k^n)^{\mathrm{T}}\right]^{\mathrm{T}}$, and $Q = \mathrm{diag}\{q_1, \dots, q_N\} \in \mathbb{R}^{N\times N}$. The state of each unit may not be fully measurable, such that we have limited access to only the output $y_k = (I_N \otimes C)x_k$, where $C \in \mathbb{R}^{p\times n}$.

By introducing the average state $\bar{x}_k = \sum_{i=1}^N x_k^i/N$, we define the disagreement vector $\xi_k := x_k - \mathbb{1}_N \otimes \bar{x}_k = (R \otimes I_n)x_k$, where $\mathbb{1}_N$ is the vector of all ones in $\mathbb{R}^N$ and $R = I_N - \mathbb{1}_{\mathbb{N}}\mathbb{1}_N^{\mathrm{T}}/N$ is the projector from $\mathbb{R}^N$ to $\mathbb{1}_N^{\perp}$. Hence, the disagreement dynamics is

$$\xi_{k+1} = (R \otimes F - L \otimes \Gamma)\xi_k + RQ \otimes B\eta_k. \tag{3}$$

We assume that the network topology is undirected so that L is a positive semi-definite symmetric matrix, whose elements on the diagonal are non-negative and those off the diagonal are non-positive [32]. We order the eigenvalues of L in an increasing order, such that $\lambda_1 = 0$ is the eigenvalue corresponding to the eigenvector $v_1 = \mathbb{1}_{\mathbb{N}}/\sqrt{N}$ and $0 \le \lambda_2 \le \dots \lambda_N$. In general, the network can be weighted so that the value of the elements off-the diagonal do not need to be zero or minus one. We do not impose that F is stable, thereby encompassing the classical consensus problems, where F is scalar and equal to one [34]. Instead, we hypothesize that F, L, and Γ are such that the spectral radius of $(R\otimes F - L\otimes\Gamma)$ is less than one, thereby leading to an asymptotically stable disagreement dynamics in the absence of noise. This will, in turn, lead to a covariance matrix $\Xi_k^Q = \mathrm{E}[\xi_k\xi_k^{\mathrm{T}}]$ that will converge to a finite steady-state matrix Ξ_∞^Q [35], where $\mathrm{E}[\cdot]$ is used to denote expectation with respect to the σ-algebra associated with the added noise to an otherwise deterministic system.

To compute closed-form expressions for the steady-state covariance, we apply the similarity transformation $(V^{\mathrm{T}} \otimes I_n)$, where V is assembled by juxtaposing column-wise the orthonormal eigenvectors of L. The modal dynamics $\zeta_k = (V^{\mathrm{T}} \otimes I_n)\xi_k$ has the following block-diagonal form:

$$\zeta_{k+1} = (V^{\mathrm{T}}RV \otimes F - \Lambda \otimes \Gamma)\zeta_k + (V^{\mathrm{T}}RQ \otimes B)\eta_k, \tag{4}$$

where $\Lambda = V^{\mathrm{T}}LV = \mathrm{diag}\{\lambda_1, \dots, \lambda_N\}$. Note that $V^{\mathrm{T}}RV$ is the identity matrix with the first element set to zero and that $V^{\mathrm{T}}R$ collates the eigenvectors of L row-wise, except for the first row that is null. Utilizing $(\cdot)_i$ to isolate the i-th n-dimensional block of a vector in $\mathbb{R}^{nN}$, we have that (4) becomes

$$(\zeta_{k+1})_1 = 0 \tag{5a}$$

$$(\zeta_{k+1})_r = (F - \lambda_r\Gamma)(\zeta_k)_r + \sum_{s=1}^N q_s v_{rs} B\eta_k \tag{5b}$$

for $r = 2, \dots, N$, where v_{rs} be the s-th component of the r-th eigenvector of L, associated with eigenvalue λ_r. Equation (5a) indicates that, irrespective of the added noise, the modal dynamics along the first modal coordinate is identically equal to zero, while the others in (5b) are modulated by the spectral properties of L (through both the eigenvalues and eigenvectors) and the internal dynamics.

III. Vulnerability of the network dynamical system to targeted attacks

To pinpoint the most influential or key nodes in the network, we consider an ideal experiment where noise is only injected at one unit, such that $Q = \mathbb{e}_i\mathbb{e}_i^{\mathrm{T}}$; $\mathbb{e}_i$ is the i-th unit vector of the natural basis of $\mathbb{R}^N$, specifying that the noise is selectively injected only at the i-th node. We evaluate the impact of the added noise on the network output by computing the steady-state covariance of the entire disagreement dynamics $\Xi_\infty^{\mathbb{e}_i\mathbb{e}_i^{\mathrm{T}}} = \lim_{k\to+\infty} \mathrm{E}\left[\xi_k\xi_k^{\mathrm{T}}\right]$.

To this aim, we examine the modal dynamics in (5), which has a simpler block-diagonal structure. Specifically, we start by computing the steady-state covariance matrix $\widetilde{\Xi}_\infty^{\mathbb{e}_i\mathbb{e}_i^{\mathrm{T}}} = \lim_{k\to+\infty} \mathrm{E}\left[\zeta_k\zeta_k^{\mathrm{T}}\right]$ of the modal dynamics. Denoting with vec and vec^{-1} the vectorization operator and its inverse[1], respectively, we can show that $\widetilde{\Xi}_\infty^{\mathbb{e}_i\mathbb{e}_i^{\mathrm{T}}}$ admits the following block-form solution in terms of the individual node dynamics and of the network topology:

Lemma 1. *Let v_{sr} be the r-th component of the s-th eigenvector of L, associated with eigenvalue λ_s. The steady-state of the N^2 blocks of size $n \times n$ of $\widetilde{\Xi}_\infty^{\mathbb{e}_i\mathbb{e}_i^{\mathrm{T}}}$ is given by*

$$\left(\widetilde{\Xi}_\infty^{\mathbb{e}_i\mathbb{e}_i^{\mathrm{T}}}\right)_{1s} = \left(\widetilde{\Xi}_\infty^{\mathbb{e}_i\mathbb{e}_i^{\mathrm{T}}}\right)_{s1} = 0, \quad s = 1, \dots, N, \tag{6a}$$

$$\left(\widetilde{\Xi}_\infty^{\mathbb{e}_i\mathbb{e}_i^{\mathrm{T}}}\right)_{rs} = v_{ri}v_{si}\mathrm{vec}^{-1}\left[G_{rs}\mathrm{vec}\left[B\Sigma_\eta B^{\mathrm{T}}\right]\right], \quad r, s = 2, \dots, N, \tag{6b}$$

where

$$G_{rs} = (I_{n^2} - (F - \lambda_s\Gamma) \otimes (F - \lambda_r\Gamma))^{-1} \tag{7}$$

is a function of the Laplacian eigenvalues, the individual dynamics F, and the inner coupling matrix Γ.

Proof. Equation (6a) follows from (5a). Likewise, (6b) is derived by setting $q_s = 0$ for all $s \neq i$ and $q_i = 1$ in (5b), so that $(\zeta_{k+1})_r = (F - \lambda_r\Gamma)(\zeta_k)_r + v_{ri}B\eta_k$ Hence, the generic rs-th block is governed by the following dynamics:

$$\begin{aligned}(\zeta_{k+1})_r(\zeta_{k+1})_s^{\mathrm{T}} &= (F - \lambda_r\Gamma)(\zeta_k)_r(\zeta_k)_s^{\mathrm{T}}(F - \lambda_s\Gamma)^{\mathrm{T}} \\ &+ v_{ri}v_{si}B\eta_k\eta_k^{\mathrm{T}}B^{\mathrm{T}} + v_{si}(F - \lambda_r\Gamma)(\zeta_k)_r\eta_k^{\mathrm{T}}B^{\mathrm{T}} \\ &+ v_{ri}B\eta_k(\zeta_k)_s^{\mathrm{T}}(F - \lambda_s)^{\mathrm{T}}.\end{aligned} \tag{8}$$

By taking the expectation of both sides of the equation, noting that noise has zero mean, and recalling that the state at time k is independent of noise at time k, we establish

$$\begin{aligned}\left(\widetilde{\Xi}_{k+1}^{\mathbb{e}_i\mathbb{e}_i^{\mathrm{T}}}\right)_{rs} &= (F - \lambda_r\Gamma)\left(\widetilde{\Xi}_\infty^{\mathbb{e}_i\mathbb{e}_i^{\mathrm{T}}}\right)_{rs}(F - \lambda_s\Gamma)^{\mathrm{T}} \\ &+ v_{ri}v_{si}B\Sigma_\eta B^{\mathrm{T}}, \quad r, s = 2, \dots, N,\end{aligned} \tag{9}$$

Equation (9) can be transformed into a linear system by matrix vectorization, whose solution for $k \to +\infty$ is equal to

$$\mathrm{vec}\left[\left(\widetilde{\Xi}_\infty^{\mathbb{e}_i\mathbb{e}_i^{\mathrm{T}}}\right)_{rs}\right] = v_{ri}v_{si}G_{rs}\mathrm{vec}\left[B\Sigma_\eta B^{\mathrm{T}}\right], \tag{10}$$

where each of these equations identifies the effect of noise injected at the i-th node on the covariance of the r-th and s-th modal coordinates. The thesis then follows. □

[1]The inverse of the vectorization operator vec : $\mathbb{R}^{a\times b} \to \mathbb{R}^{ab}$ is the operator $\mathrm{vec}^{-1} : \mathbb{R}^{ab} \to \mathbb{R}^{a\times b}$ such that $\mathrm{vec}^{-1}(\mathrm{vec}(W)) = W$ for all $W \in \mathbb{R}^{a\times b}$ and $\mathrm{vec}(\mathrm{vec}^{-1}w) = w$ for all $w \in \mathbb{R}^{ab}$.

Remark 1. A similar decomposition for the covariance of the error dynamics in the continuous-time case is presented in equations (23) and (24) in [17].

The overall effect of noise added at node i can be quantified by computing the steady-state covariance matrix Ξ_k^∞ associated with the disagreement vector, similar to [17]–[19]. Such a matrix is given block-wise in terms of the modal matrices in Lemma 1, as

$$\left(\Xi_\infty^{\mathfrak{e}_i\mathfrak{e}_i^{\mathrm{T}}}\right)_{hj} = \sum_{r=2}^{N}\sum_{s=2}^{N} v_{lh}v_{rj}\left(\widetilde{\Xi}_\infty^{\mathfrak{e}_i\mathfrak{e}_i^{\mathrm{T}}}\right)_{rs}. \tag{11}$$

We propose to study causal influence in terms of the vulnerability of the entire system to noise injected at the i-th node. Specifically, we introduce a vulnerability index to quantify the overall effect of adding noise to a specific node on a weighted combination of the disagreement of the units' outputs.

In quantitative terms, the vulnerability index is

$$\mathrm{Vul}(i,M) = \mathrm{Tr}\left[(M^{\mathrm{T}}\otimes C)\Xi_\infty^{\mathfrak{e}_i\mathfrak{e}_i^{\mathrm{T}}}(M\otimes C^{\mathrm{T}})\right], \tag{12}$$

where $M = \mathrm{diag}\{m_1,\dots,m_N\} \in \mathbb{R}^{N\times N}$ is a diagonal matrix that is used to weight the relevance of each network node. For example, M can be chosen with larger diagonal entries corresponding to nodes which are deemed to be more critical in the network, so that their covariance must be contained, potentially at the expense of the other nodes. If $M = I_N$, all nodes are equally treated in the definition of the vulnerability index; this choice is typically employed in the formulation of performance matrices for the study of leadership and robustness in network control systems [17]–[19].

We establish the following result, highlighting the interplay between the individual dynamics and the Laplacian eigenvalues and eigenvectors on vulnerability:

Proposition 1. *The vulnerability index for node i in equation* (12) *can be expressed as*

$$\begin{aligned}\mathrm{Vul}(i,M) = \sum_{j=1}^{N} m_j^2 \sum_{r=2}^{N}\sum_{s=2}^{N} v_{rj}v_{sj}v_{si}v_{ri} \\ \mathrm{Tr}\left(C\mathrm{vec}^{-1}\left[G_{rs}\mathrm{vec}\left[B\Sigma_\eta B^{\mathrm{T}}\right]\right]C^{\mathrm{T}}\right),\end{aligned} \tag{13}$$

where the spectral properties of L enter matrix G_{rs} in (7)*.*

Proof. To obtain the vulnerability index, we need to compute the trace of

$$\Upsilon_M(i) = (M^{\mathrm{T}}\otimes C)\Xi_\infty^{\mathfrak{e}_i\mathfrak{e}_i^{\mathrm{T}}}(M\otimes C^{\mathrm{T}}), \tag{14}$$

which is the sum of the traces of its N blocks along the diagonal $\left(\Upsilon_M(i)\right)_{11},\dots,\left(\Upsilon_M(i)\right)_{NN}$. The generic j-th block takes the form

$$\left(\Upsilon_M(i)\right)_{jj} = m_j^2 C\left(\Xi_\infty^{\mathfrak{e}_i\mathfrak{e}_i^{\mathrm{T}}}\right)_{jj}C^{\mathrm{T}}. \tag{15}$$

From Lemma 1 and equation (11), we establish

$$\left(\Xi_\infty^{\mathfrak{e}_i\mathfrak{e}_i^{\mathrm{T}}}\right)_{jj} = \sum_{r=2}^{N}\sum_{s=2}^{N} v_{rj}v_{sj}v_{si}v_{ri}\mathrm{vec}^{-1}\left[G_{rs}\mathrm{vec}\left[B\Sigma_\eta B^{\mathrm{T}}\right]\right]. \tag{16}$$

Combining (15) and (16) yields

$$\begin{aligned}\left(\Upsilon_M(i)\right)_{jj} = m_j^2\sum_{r=2}^{N}\sum_{s=2}^{N} v_{rj}v_{sj}v_{si}v_{ri} \\ C\mathrm{vec}^{-1}\left[G_{rs}\mathrm{vec}\left[B\Sigma_\eta B^{\mathrm{T}}\right]\right]C^{\mathrm{T}}.\end{aligned} \tag{17}$$

Applying the trace operator and summing for j that goes from 1 to N yields the claim. □

Remark 2. Equation (16) confirms the intuition that injecting noise at one node influences the steady-state covariance of any other node. The extent of this effect depends on the network topology and the individual dynamics, similar to observations for a wide range of perturbations in biological networks [36]. In particular, the effect of noise injected at node i on node j is controlled by the i- and j-th components of all the Laplacian eigenvectors (except of the first ones), the entire Laplacian spectrum, and internal dynamics.

Remark 3. When all the nodes are equivalently weighted in the vulnerability index ($M = I_N$), equation (13) reduces to

$$\mathrm{Vul}(i,I_N) = \sum_{r=2}^{N} v_{ri}^2\,\mathrm{Tr}\left(C\mathrm{vec}^{-1}\left[G_{rr}\mathrm{vec}\left[B\Sigma_\eta B^{\mathrm{T}}\right]\right]C^{\mathrm{T}}\right), \tag{18}$$

where we leveraged the fact that the eigenvectors are orthonormal. This equation shows that the effect of noise injected at node i is modulated by all the Laplacian eigenvalues (entering the equation through G_{rr}), each weighted by the i-th component of the corresponding eigenvector.

IV. Inference of Causal Influence from Real Experimental Observations

In a real experiment, it is impossible to manipulate the pattern of the added noise, as required by the ideal experiments underlying the computation of the vulnerability index (12). In general, noise in a real experiment will affect all the nodes in the network, rather than a single one. Likewise, the researcher has no knowledge about the network topology and the individual dynamics, thereby hindering any attempt to estimate the vulnerability index in (12). The researcher has only access to the time-series of the individual units, from which he/she could compute the covariance matrix $\Sigma_k^Q = \lim_{t\to+\infty}\mathrm{E}\left[y_k y_k^{\mathrm{T}}\right]$ of the network output y_k. Here, we demonstrate that such a matrix could suffice to infer salient information about network vulnerability, that is, to pinpoint the nodes from which a targeted attack would produce the largest effect on the overall system dynamics.

The reason why the real and the ideal experiments can be reconciled is due to the two classical principles in circuit theory [37] that carry over to the context of network dynamical systems. First, due to the linearity of the model, the response of the system to noise injected at all nodes can be obtained as the sum of the responses to noise individually injected at each of the nodes. Hence, the real experiment can be regarded as the superposition of N ideal experiments, in which noise is selectively injected at a different node:

$$\Xi_\infty^Q = \sum_{j=1}^{N} q_j^2\Xi_\infty^{\mathfrak{e}_j\mathfrak{e}_j^{\mathrm{T}}}. \tag{19}$$

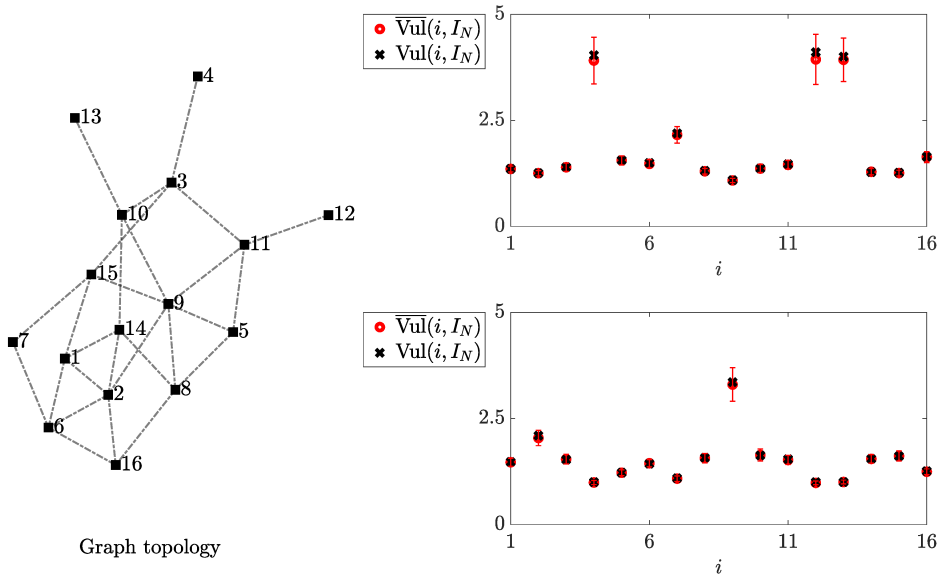

Fig. 2. Illustration of the approach on scalar dynamics. Network topology from [18] (left panel). Comparison between the estimation of the vulnerability index through (21) in Proposition 3 and the exact value in (30) for each node, with $Q = M = I_N$: classical consensus (top-right panel) and stable dynamics (bottom-right panel). Mean sample covariances are computed using $T = 1,000$ time-steps and error bars show one standard deviation with respect to 100 realizations.

Second, the principle of reciprocity extends to network dynamical systems, whereby the effect of noise injected at node i on node j is equivalent to the effect of noise injected at node j on node i.

Proposition 2 (Reciprocity principle)**.** *For all* $i, j = 1, \dots, N$,

$$\left(\Xi_\infty^{\mathfrak{e}_i \mathfrak{e}_i^{\mathrm{T}}}\right)_{jj} = \left(\Xi_\infty^{\mathfrak{e}_j \mathfrak{e}_j^{\mathrm{T}}}\right)_{ii} \tag{20}$$

Proof. The claim follows by simply noting that swapping subscripts i and j in (16) does not change the result. □

By applying the linearity and the reciprocity principles, we can exactly infer the vulnerability index when matrix M, weighting the relevance of each node, coincides with matrix Q, measuring the strength of the noise added to the network nodes. In this case, the vulnerability index for each node can be assessed from the covariances associated with the network output y_k, as demonstrated in the following proposition:

Proposition 3. *If* $M = Q$*, then, for all* $i = 1, \dots, N$*, the vulnerability index defined in* (12) *can be computed as*

$$\mathrm{Vul}(i, M) = \mathrm{Tr}\left((R \otimes I_p)\Sigma_\infty^Q (R \otimes I_p)\right)_{ii}. \tag{21}$$

Proof. We start by observing that, from the superposition principle expressed in (19), the i-th diagonal block of Ξ_∞^Q can be written as

$$\left(\Xi_\infty^Q\right)_{ii} = \sum_{j=1}^{N} q_j^2 \left(\Xi_\infty^{\mathfrak{e}_j \mathfrak{e}_j^{\mathrm{T}}}\right)_{ii} \tag{22}$$

Using the reciprocity principle in Proposition 2, for all j, we replace the i-th diagonal block of $\Xi_\infty^{\mathfrak{e}_j \mathfrak{e}_j^{\mathrm{T}}}$ with the j-th diagonal block of $\Xi_\infty^{\mathfrak{e}_i \mathfrak{e}_i^{\mathrm{T}}}$ to obtain

$$\begin{aligned}\left(\Xi_\infty^Q\right)_{ii} &= \sum_{j=1}^{N} q_j^2 \left(\Xi_\infty^{\mathfrak{e}_i \mathfrak{e}_i^{\mathrm{T}}}\right)_{jj} \\ &= \sum_{j=1}^{N} q_j^2 \sum_{r=2}^{N} \sum_{s=2}^{N} v_{rj} v_{sj} v_{si} v_{ri} \mathrm{vec}^{-1}\left[G_{rs} \mathrm{vec}\left[B \Sigma_\eta B^{\mathrm{T}}\right]\right],\end{aligned} \tag{23}$$

for all $i = 1, \dots, N$.

Next, note that

$$(R \otimes I_p)\Sigma_\infty^Q (R \otimes I_p) = (I_N \otimes C)\Xi_\infty^Q (I_N \otimes C^{\mathrm{T}}) \tag{24}$$

and, therefore,

$$(R \otimes I_p)\Sigma_\infty^Q (R \otimes I_p)_{ii} = C \left(\Xi_\infty^Q\right)_{ii} C^{\mathrm{T}}. \tag{25}$$

Combining (23) and (25) yields

$$\begin{aligned}&(R \otimes I_p)\Sigma_\infty^Q (R \otimes I_p)_{ii} \\ &= \sum_{j=1}^{N} q_j^2 \sum_{r=2}^{N} \sum_{s=2}^{N} v_{rj} v_{sj} v_{si} v_{ri} C \mathrm{vec}^{-1}\left[G_{rs} \mathrm{vec}\left[B \Sigma_\eta B^{\mathrm{T}}\right]\right] C^{\mathrm{T}}.\end{aligned} \tag{26}$$

Since $M = Q$, applying the trace operator and using Proposition 1, one obtains that, for all $i = 1, \dots, N$,

$$\mathrm{Tr}\left((R \otimes I_p)\Sigma_\infty^Q (R \otimes I_p)\right)_{ii} = \mathrm{Vul}(i, M). \tag{27}$$

□

Remark 4. The claim of Proposition 3 can be generalized to the case when Q and M are full matrices, with elements outside the diagonal. Equation (27) would carry over in this more general case, provided that $Q = M$. The technical proof is rather different, whereby the elegant application of the reciprocity principle would not be sufficient; the proof of this claim is in the Appendix.

Remark 5. The case considered in Remark 4 of Q and M non-diagonal matrices can be elaborated further by examining the instance in which Q commutes with the Laplacian matrix

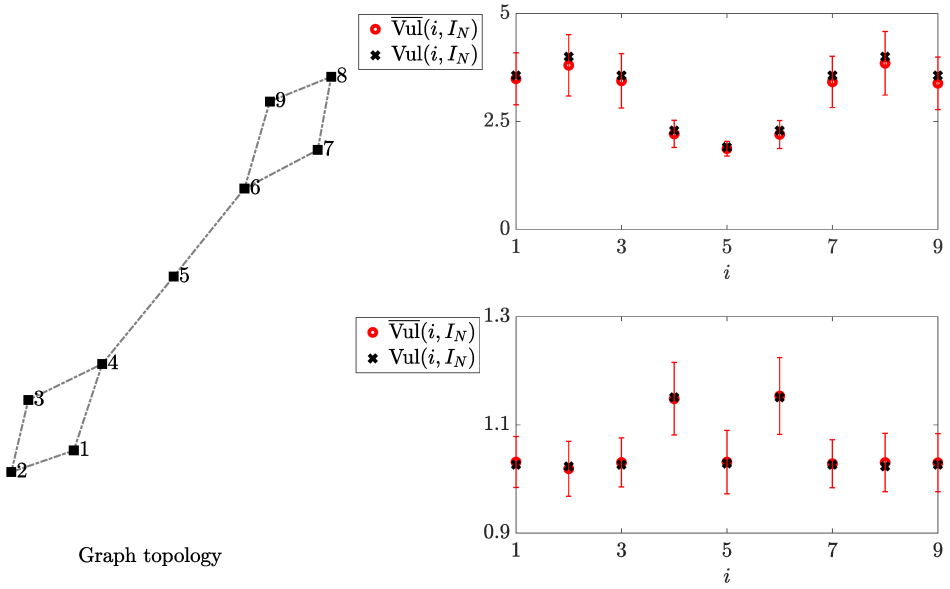

Fig. 3. Illustration of the approach on scalar dynamics. Network topology constituted by two cliques separated by a cut vertex (left panel). Comparison between the estimation of the vulnerability index through (21) in Proposition 3 and the exact value in (30) for each node, with $Q = M = I_N$: classical consensus (top-right panel) and stable dynamics (bottom-right panel). Mean sample covariances are computed using $T = 1,000$ time-steps and error bars show one standard deviation with respect to 100 realizations.

of the network (that is, $[Q, L] = 0$). Under this assumption, it is possible to construct lower and upper bounds for $\mathrm{Vul}(i, I_N)$ in terms of the spectral properties of Q,

$$\begin{aligned} \mathrm{Vul}(i, I_N) &\leq \frac{\mathrm{Tr}\left((R \otimes I_n)\Sigma_\infty^Q (R \otimes I_n)\right)_{ii}}{\theta_2^2}, \\ \mathrm{Vul}(i, I_N) &\geq \frac{\mathrm{Tr}\left((R \otimes I_n)\Sigma_\infty^Q (R \otimes I_n)\right)_{ii}}{\theta_{\max}^2}. \end{aligned} \tag{28}$$

where θ_2 and $\theta_{\max}$ are the smallest non-zero and largest eigenvalues of Q. For $Q = M = I_N$, the two bounds coincide and they match (21). The proof of this claim is in the Appendix.

V. Illustration of the approach on synthetic data

We consider the cases of scalar and second-order dynamics to demonstrate the applicability of the approach for different individual dynamics. For scalar dynamics, we further detail the validity of the approach against parameter variations and across different network topologies. Toward real applications, we simply rely on the time-series of the nodes, which we assume evolve under the influence of standard white Gaussian noise ($\Sigma_\eta = 1$).

Throughout the analysis, we assume to have access to $T = 1,000$ time-steps for the output of each node, from which we calculate the disagreement with respect to the average. We repeat the analysis 100 times from randomly generated initial conditions. From these time-series, we compute the covariances of the disagreement dynamics, which are required to estimate the vulnerability metric through (21) in Proposition 3 or to establish conservative bounds via (28). Specifically, for each realization, we compute sample means for all quantities and we then use these quantities to quantify variability across realizations through standard deviation. For clarity, we use a superimposed bar to indicate the estimation of the covariances from time-series, and the consequent inferences on vulnerability.

A. Scalar dynamics

We start the analysis with scalar dynamics, with $F = \alpha$, $\Gamma = \beta$, $B = 1$, $C = 1$, for which the disagreement dynamics is asymptotically stable if $|\ \alpha - \beta\lambda_i\ | < 1$ for $i = 2, \dots, N$ and the matrix G_{rr} in (6) becomes

$$G_{rr} = \frac{1}{1 - (\alpha + \beta w_r)^2}. \tag{29}$$

Hence, the vulnerability index (12) for $M = Q = I_N$ is

$$\mathrm{Vul}(i, I_N) = \sum_{r=2}^{N} \frac{v_{ri}^2}{1 - (\alpha + \beta w_r)^2}. \tag{30}$$

We begin with the study of the 16-node network examined in [18], whose nodes have degree varying from one to six and $0.609 \leq \lambda_i \leq 8.03$ for $i = 2, \dots, N$. We select two possible combinations for (α, β), which beget the same spectral radius of $(R \otimes F - L \otimes \Gamma)$: $(1.000, 0.159)$ and $(-0.100, 0.100)$. The first configuration corresponds to the classical consensus problem with marginally stable individual dynamics, while the second one has a stable, yet oscillating, individual dynamics. In Table I, we report the vulnerability at each node (30) in the two cases, as a function of several measures of centrality, including the degree, the betweenness centrality, the closeness centrality, the centrality measure by [38], and the eccentricity. For the case of consensus, the degree centrality offers the best proxy of vulnerability (Pearson correlation coefficient of -0.91), such that the nodes with the lowest degree are the most influential. On the other hand, in the other case of stable dynamics, the best proxy is the centrality measure by [38] (Pearson correlation coefficient of 0.89), such that nodes with higher centrality are more influential. These findings echoe previous results on continuous-time systems [13], [17], suggesting that dynamics play a critical role in defining vulnerability to targeted attacks.

Figure 2 compares the estimation of the vulnerability index for each node, from time-series through (21) in Proposition

	Nodes															
	1	**2**	**3**	**4**	**5**	**6**	**7**	**8**	**9**	**10**	**11**	**12**	**13**	**14**	**15**	**16**
$\deg(i)$	4	5	4	1	3	4	2	4	6	4	4	1	1	4	4	3
$\mathrm{bc}(i)$	5.97	12.30	21.07	0	2.63	4.90	1.87	8.33	30.83	20.07	18.37	0	0	9.13	18.20	2.33
$10^2 \times \mathrm{cc}(i)$	3.13	3.33	3.23	2.22	3.13	2.78	2.63	3.13	4.00	3.33	3.13	2.17	2.27	3.23	3.45	2.56
$10 \times \mathrm{cg}(i)$	1.74	2.01	1.66	0.49	1.45	1.50	0.95	1.87	3.07	1.73	1.54	0.48	0.49	1.93	1.98	1.33
$\mathrm{e}(i)$	4	4	4	5	3	4	4	4	3	3	3	4	4	4	3	5
$\mathrm{Vul}(i, I_N)^\star$	1.36	1.26	1.40	4.04	1.56	1.50	2.20	1.31	1.09	1.37	1.47	4.11	4.00	1.28	1.27	1.65
$\mathrm{Vul}(i, I_N)^{\star\star}$	1.48	2.10	1.53	1.00	1.22	1.43	1.09	1.58	3.36	1.63	1.54	1.00	1.00	1.55	1.61	1.25

TABLE I

CENTRALITY AND VULNERABILITY: TOPOLOGY FROM [18]. ROWS FROM 3 TO 7 ROWS REPORTS, FOR EACH NODE $i = 1, \ldots, 16$, THE DEGREE CENTRALITY $\deg(i)$, BETWEENNESS CENTRALITY $\mathrm{bc}(i)$, CLOSENESS CENTRALITY $\mathrm{cc}(i)$, CENTRALITY $\mathrm{cg}(i)$ AS DEFINED IN [38], RESPECTIVELY. THE LAST TWO ROWS REPORT THE VULNERABILITY INDEX FOR CLASSICAL CONSENSUS CASE AND STABLE DYNAMICS, IDENTIFIED BY ONE AND TWO STARS, RESPECTIVELY.

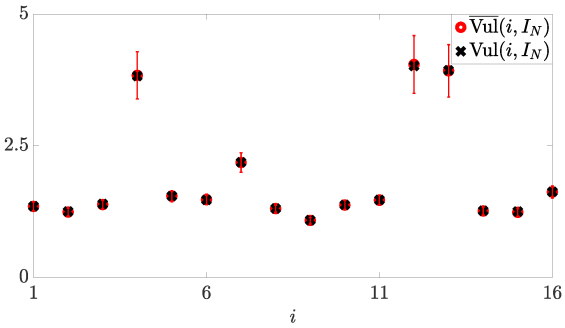

Fig. 4. Robustness of the approach to perturbation of nodal parameters. Scalar consensus dynamics and network topology from [18]. Comparison between the estimation of the vulnerability index through (21) in Proposition 3 and the exact value for each node, with $Q = M = I_N$. Mean sample covariances are computed using $T = 1,000$ time-steps, and error bars show one standard deviation with respect to 100 realizations.

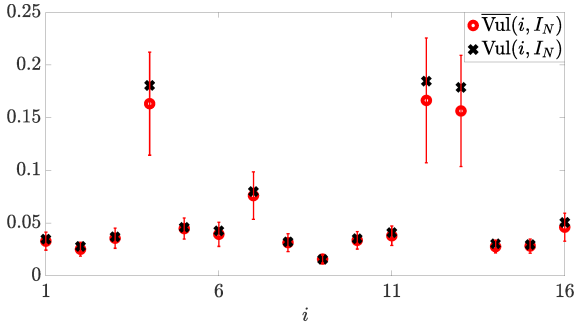

Fig. 5. Illustration of the approach on second-order dynamics. Network topology from [18]. Comparison between the estimation of the vulnerability index through (21) in Proposition 3 and the exact value for each node, with $Q = M = I_N$. Mean sample covariances are computed using $T = 1,000$ time-steps, and error bars show one standard deviation with respect to 100 realizations.

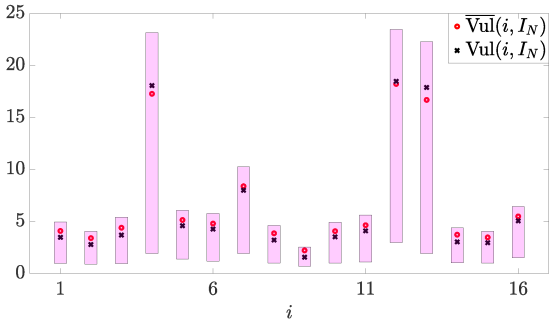

Fig. 6. Illustration of the approach on second-order dynamics. Network topology from [18]. Comparison between the estimation of the vulnerability index through bounds in (28) and the exact value for each node, with $Q = I_N + 0.05L$ and $M = I_N$. For each node, we report the mean of the numerator of (28) from the 100 realizations, and we use a bar to mark the range of the bounds accounting for one standard deviation from the mean.

3, against the true value in (30) for the possible parameter combinations. In both cases, we can accurately locate the most influential nodes in the network from the time-series of real experimental observations. Importantly, the variation across observations is small with respect to the variation among the values of the vulnerability index for different nodes, such that, in principle, a single observation could suffice to correctly infer the most influential nodes in the network.

To test the efficacy of the approach on other network topologies, we also examine a topology composed of two four-node cliques joint by one cut vertex. We confirm the accuracy of the approach in detecting the most influential nodes, as shown in Figure 3. Interestingly, the relationship between vulnerability and degree centrality is consistent across network topologies, but the best topological proxies to identify key players are different, as reported in Table II. For the case of consensus, betweenness centrality is the best proxy (Pearson correlation coefficient of -0.99), while for the other case, the degree centrality offers the best representation (Pearson correlation coefficient of 1.00).

To delve into the robustness of the inference with respect to parameter variations, we focus on consensus over the 16-node network. For each node, we select the scalar parameters α and B uniformly in the interval $[0.995, 1.005]$. Figure 4 confirms excellent matching between the vulnerability computed according to equation (12), and our estimation performed using (21). The observed robustness against parameter variation is due to the continuous dependence of the states' evolution on the parameters of the network dynamical system.

B. Second-order dynamics

We now consider a second-order discrete-time consensus protocol, with

$$F = \begin{bmatrix} 1 & \tau \\ 0 & 1 - p_0\tau \end{bmatrix}, \Gamma = c \begin{bmatrix} 0 & 0 \\ p_1\tau & p_2\tau \end{bmatrix}, B = \begin{bmatrix} 0 \\ 1 \end{bmatrix}. \quad (31)$$

The characteristic time $\tau = 0.2$, and the parameters $p_0 = p_1 = 1$ and $p_2 = 2$ are selected according to [39], and c is selected as 0.14 to ensure asymptotic stability of the disagreement dynamics. Further, we consider that only the first state variable is measured, that is, $C = [1\ 0]$.

Figure 5 confirms the results of the classical consensus protocol, such that, when $M = I_N$, the system is most vulnerable to noise added to the node with the lowest degree. This fact is well captured by the estimation of the vulnerability index for $Q = M = I_N$ from time-series through (21) in Proposition 3.

	Nodes								
	1	**2**	**3**	**4**	**5**	**6**	**7**	**8**	**9**
$\deg(i)$	2	2	2	3	2	3	2	2	2
$\mathrm{bc}(i)$	3.00	0.50	3.00	15.50	16.00	15.50	3.00	0.50	3.00
$10^2 \times \mathrm{cc}(i)$	4.55	3.70	4.55	5.88	6.25	5.88	4.55	3.70	4.55
$10 \times \mathrm{cg}(i)$	0.73	0.66	0.73	1.02	1.86	1.02	0.73	0.66	0.73
e(i)	5	6	5	4	3	4	5	6	5
$\mathrm{Vul}(i, I_N)^\star$	3.57	4.00	3.57	2.29	1.91	2.29	3.57	4.00	3.57
$\mathrm{Vul}(i, I_N)^{\star\star}$	1.03	1.02	1.03	1.15	1.02	1.15	1.03	1.02	1.03

TABLE II

CENTRALITY AND VULNERABILITY: TOPOLOGY FROM FIGURE 3, LEFT PANEL. ROWS FROM 3 TO 7 ROWS REPORTS, FOR EACH NODE $i = 1, \ldots, 16$, THE DEGREE CENTRALITY $\deg(i)$, BETWEENNESS CENTRALITY $\mathrm{bc}(i)$, CLOSENESS CENTRALITY $\mathrm{cc}(i)$, CENTRALITY $\mathrm{cg}(i)$ AS DEFINED IN [38], RESPECTIVELY. THE LAST TWO ROWS REPORT THE VULNERABILITY INDEX FOR CLASSICAL CONSENSUS AND STABLE DYNAMICS, IDENTIFIED BY ONE AND TWO STARS, RESPECTIVELY.

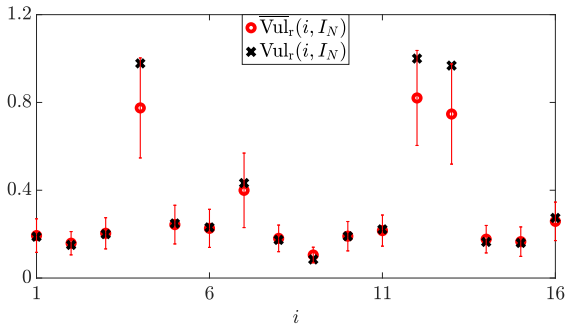

Fig. 7. Illustration of the approach on second-order dynamics. Network topology from [18]. Comparison between the estimation of the vulnerability index through bounds in (28) and the exact value for each node, with $Q = I_N + 0.05L$ and $M = I_N$. For each node, we report the vulnerability ratio (32) and the mean of its estimation using the bounds in (28) from the 100 realizations. The error bars show one standard deviation with respect to 100 realizations.

The numerical estimation from a real experimental observation can be used to faithfully reproduce the vulnerability node rank.

Next, we consider the case in which the noise affects the system dynamics in a more complex manner, according to $Q = I_N + 0.05L$. Such a choice models combination of disturbances that are added to both the nodes and the edges of the network. In this case, $M \neq Q$, so that we cannot apply Proposition 3 and we should resort to the bounds in (28). As shown in Figure 5, these bounds offer a conservative estimate of the vulnerability index, which could be heuristically utilized to understand causal influence within the network dynamical system. The wide range between the upper and lower bounds are due to the spread in the spectrum of L, such that $\lambda_2 = 0.61$ and $\lambda_N = 8.03$. However, the main goal of our analysis is to identify the key nodes for network vulnerability, rather than the exact estimate of the vulnerability index. Therefore, the bounds should rather be used to estimate the vulnerability ratio

$$\mathrm{Vul}_\mathrm{r}(i, I_N) = \frac{\mathrm{Vul}(i, I_N)}{\max_i \mathrm{Vul}(i, I_N)}, \tag{32}$$

and correctly rank the importance of the nodes in the network, see Figure 7.

VI. ILLUSTRATION OF THE APPROACH ON REAL-WORLD DATASETS

Upon validating the methodology on synthetic data, we illustrate the use of our method on two examples of collective dynamics, in which it is critical to identify influential nodes from time-series. In both examples, we assume that noise enters each unit in the same manner ($Q = I_N$) and that each node is equally important in the network ($M = I_N$). Accordingly, the vulnerability index will be computed from Proposition 3.

A. Firearm prevalence in the United States of America

We demonstrate the approach on the firearm prevalence dataset by [40], which established information-theoretic tools to examine the key drivers of firearm acquisition in the aftermath of mass shootings. In these efforts, firearm acquisition is estimated from the time-series of background checks per capita for each of the 50 states in the United States of America at a monthly resolution from 1999 to 2017. The National Instant Criminal Background Check System was implemented in November 1998 and permits authorized sellers to assess whether a prospective buyer is eligible for the purchase of a firearm. Recent findings from [41] point at an underlying network structure to firearm prevalence in the United States of America, whereby firearm acquisitions in any State are influenced by acquisition in other States.

Here, we seek to further delve into this collective dynamics to identify the most influential States, whose firearm prevalence has a stronger impact in Nation-wide sales. The time-series of background checks are characterized by strong tendency and seasonal effects, whereby we are always witnessing a continuous surge in firearm acquisition that has two peaks toward the end of the year and in Spring. To mitigate these non-stationary phenomena, the time-series can be seasonally adjusted and detrended using ad-hoc econometric tools, as detailed in [40].

We calculate the sample mean covariance matrix associated with these detrended and seasonally-adjusted time-series. From the analysis, we exclude Connecticut and Hawaii, since Connecticut did not report background checks for almost two years of zero, and Hawaii always reported zero background checks except of one month in nearly 20 years, and we estimate the vulnerability index at the state in (21) from Proposition 3. States with a high value of this metric should be those at which an applied disturbance will cause the strongest effect on the entire Country. As shown in Figure 8, the five (top 10%) most influential states are South Dakota, Tennessee, Alaska, Alabama, and Colorado.

A potential mechanism that could underpin the higher influence of these States might be sought in the restrictiveness of firearm regulation. As proposed in [40], this variable can be quantified in terms of the fraction of firearm safety laws in effect over a total of 133 possible laws between 1999

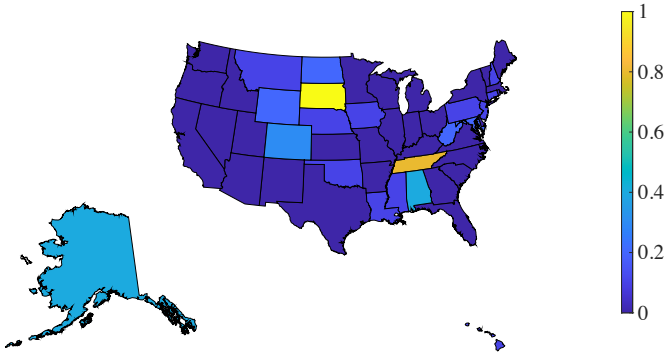

Fig. 8. Estimated vulnerability index for each State for the dataset of background checks in the United States of America from 1999 to 2017. Values are computed from detrended and deseasonalized time-series in [40]. Data are normalized between 0 and 1.

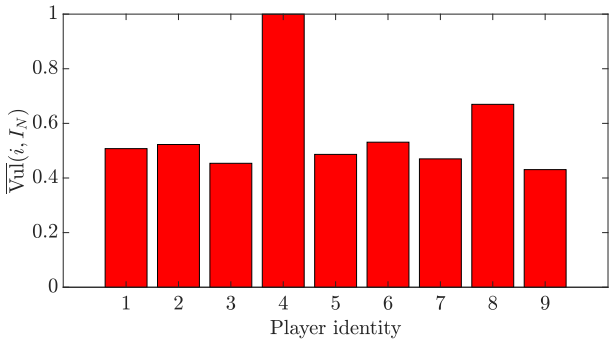

Fig. 9. Estimated vulnerability index for each of the nine players of the soccer team dataset in [42]. Values are normalized between 0 and 1.

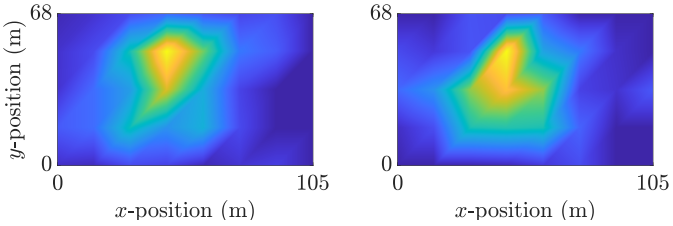

Fig. 10. Heat maps for the position distribution of players 4 (left panel) and 8 (right panel) on the soccer field of the soccer team dataset in [42]. The positional frequency of the players on the field increases as the color changes from dark blue to light yellow, so that player 4 is a playmaker and 8 a striker. The team is attacking from right to left, such that their goal line is at $x = 105\,\mathrm{m}$ and they should score by attacking the goal line of their opponents at $x = 0\,\mathrm{m}$.

and 2017, ranging from 0.752 for Massachusetts (the most restrictive State) to 0.052 for Vermont (the most permissive State). It is tenable that States in which it is easier to purchase a firearm might have a higher connectivity in the network, whereby other States may use them as proxy of potential changes in firearm regulations that could then reverberate into stricter policies in the entire Country. Indeed, from a k-means analysis with $k = 2$, we found the cluster of the most influential states (South Dakota, Tennessee, Alaska, and Alabama) to be a proper subset of that of the most permissive states identified in [41].

B. Analysis of a soccer dataset

Next, we demonstrate the approach in the different context of team sport. Specifically, we examine a dataset consisting of the positions of nine (out of eleven) soccer players of a Norwegian team in a soccer game [42]. The players' motion is scored in terms of their planar position on the soccer field in pixels, sampled at 2 Hz. For each player, we focus on the time-series of the speed from [43], as a movement metric that could be used to capture coordination in the team. Then, we estimate the vulnerability index using (21), to ascertain the influence of the player on the group. In this context, vulnerability is associated with the lack of coordination among the team players.

Figure 9 shows that the two key players in the team are number 4 and 8. From the heat maps of the position densities displayed in Figure 10, we identify that player 4 acts behind the strikers, while number 8 is one of the two strikers. This analysis suggests that a reduction in the coordination of either of these two players could hinder the coordination of the whole team. These players likely constitute the critical offense terminals of the team who catalyze the offense strategy for the whole team and set the tempo for the attacks. It is tenable that these players might have a high degree in the network of interaction between the players, whereby teammates will often seek for them during the game for finalizing an action and circulate the ball. Notably, the key players are not those who retain the ball, but rather they belong to the cluster of players with the least ball possession. Indeed, player 4 and 8 handle the ball for the 0.57% and 0.67% of the total time, respectively, against an average of 1.02% in the team, thus pointing at the crucial role of the movements off the ball in all modern dynamic sports [44].

VII. CONCLUSIONS

A critical area of study in network dynamical systems entails the identification of influential nodes, from which it could be possible to modulate the response of the entire system. Here, we establish a novel approach to identify these key players in network dynamical systems from time-series of real experiments. We focus on synchronization problems, where a network of time-invariant, diffusively coupled linear systems synchronize against added noise. In the absence of added noise, the disagreement dynamics is assumed to be asymptotically stable, so that the units converge to a synchronous state; the presence of the added noise challenges this process. For this class of problems, the influence of a node is defined as the extent to which adding noise at that particular node affects the steady-state covariance of the disagreement dynamics, that is, the vulnerability of the network to a targeted disturbance. We demonstrate that the influence of each of the nodes can be effectively inferred without a calibrated mathematical model. By computing the covariance matrix of the disagreement dynamics from time-series of real experimental observations, in which noise plagues each of the units, we can pinpoint influential nodes, thereby reconciling ideal and real experiments.

The chief reason for the correspondence between ideal and real experiments lies in the reciprocity principle which we have discovered. Reciprocity is ubiquitous in mechanics and electromagnetics, in the form of the classical Maxwell-Betti reciprocal theorem of deflections [30], [45], Rayleigh's reciprocity theorem in acoustics [31], and Lorentz theorem in electromagnetics [46]. Not surprisingly, it extends to synchronization of coupled linear units, whereby injecting noise at

node A of a network and measuring its effect on the steady-state covariance at node B is equivalent to injecting noise at B and measuring at A. By virtue of the reciprocity theorem, each node leaves a footprint on the overall dynamics that allows for precisely deciphering its specific contribution in a causal sense. These results could beget foundational advances in both practical methodologies and theory of network dynamical systems.

For scalar and second-order dynamics, we demonstrate the accuracy of the approach in supporting the identification of influential nodes from time-series of real experimental observations. Interestingly, influence is mediated by the interplay between dynamics and topology, so that peripheral nodes may be key players in some cases and have a secondary role in others. Irrespective of the select dynamics, our approach can detect influential nodes within even a single observation. Although the correspondence between ideal and real experiments is exact only when the vulnerability index weighs each node in accordance with their corresponding added noise, we establish conservative bounds that can be used for addressing more general cases. Translating the approach to real-world applications, we examine two case problems: firearm prevalence in the United Stated of America and coordination of soccer players in a match. For both datasets, our approach highlights interesting mechanisms underlying causal influence.

An alternative approach to infer the vulnerability index $\mathrm{Vul}(i, M)$ would be to undertake the identification of the network dynamical system from the available time-series and then calculate the vulnerability using (12). A number of strategies have been proposed to address this issue, offering a comprehensive toolbox to infer topology and individual dynamics from noisy time-series [24]–[29]. These strategies should be pursued when one is interested in going beyond the identification of the key players, in search of the mechanism that underlie their differential role in the network dynamical system. Undertaking this step will bring further computational challenges and require additional hypotheses. For example, the promising and elegant approach by [28] assumes the state dynamics to be asymptotically stable, the network dynamical system to be globally minimal, measurements to be a subset of state variables, and the transfer function to be minimum phase. None of these hypotheses is needed to determine key players by using our approach, because we only require the estimation of the steady state covariance.

There are several directions along which the work can be extended. First, it should be important to devise methodologies for inferring influence from real experiments in which nodes have heterogeneous nodal dynamics and additive noises. Second, the entire methodology assumes that the network is undirected, which allows for deriving modal equations that would be not feasible in the case of directed networks. Third, the mathematical treatment is presently limited to time-invariant linear dynamics, thereby calling for further research on temporal networks and nonsmooth dynamics.

Appendix
Analysis of non-diagonal Q and M

In this more general case, the model equations are as in (2), where Q specifies how noise enters the system dynamics, and the vulnerability index is defined in (12), where M is chosen to emphasize or deemphasize parts of the system.

Proposition 4. *For arbitrary, non-diagonal M, the vulnerability index for node i can be expressed as*

$$\mathrm{Vul}(i,M) = \sum_{j=1}^{N}\sum_{r=2}^{N}\sum_{s=2}^{N} v_{ri}v_{si}\left(\sum_{t=1}^{N} v_{rt}m_{tj}\right)\left(\sum_{w=1}^{N} v_{sw}m_{wj}\right) \mathrm{Tr}\left(C\mathrm{vec}^{-1}\left[G_{rs}\mathrm{vec}\left[B\Sigma_\eta B^{\mathrm{T}}\right]\right]C^{\mathrm{T}}\right), \tag{33}$$

where the Laplacian eigenvalues modulate the elements of the matrix G_{rs} in (7)*.*

Proof. The generic j-th diagonal block of $\Upsilon_M(i)$ in (14) takes the form

$$\left(\Upsilon_M(i)\right)_{jj} = \sum_{t=1}^{N}\sum_{w=1}^{N} m_{tj}m_{wj}C\left(\Xi_\infty^{\mathbb{e}_i\mathbb{e}_i^{\mathrm{T}}}\right)_{tw}C^{\mathrm{T}}. \tag{34}$$

From Lemma 1, and transforming back from the modal coordinates to the original coordinates, we obtain

$$\left(\Xi_\infty^{\mathbb{e}_i\mathbb{e}_i^{\mathrm{T}}}\right)_{tw} = \sum_{r=2}^{N}\sum_{s=2}^{N} v_{rt}v_{sw}v_{si}v_{ri}\mathrm{vec}^{-1}\left[G_{rs}\mathrm{vec}\left[B\Sigma_\eta B^{\mathrm{T}}\right]\right]. \tag{35}$$

Combining (34) and (35) yields

$$\begin{aligned}\left(\Upsilon_M(i)\right)_{jj} &= \sum_{t=1}^{N}\sum_{w=1}^{N} m_{tj}m_{wj}\sum_{r=2}^{N}\sum_{s=2}^{N} v_{lt}v_{rw}v_{si}v_{ri} \\ &\quad C\mathrm{vec}^{-1}\left[G_{rs}\mathrm{vec}\left[B\Sigma_\eta B^{\mathrm{T}}\right]\right]C^{\mathrm{T}} \\ &= \sum_{r=2}^{N}\sum_{s=2}^{N} v_{ri}v_{si}\left(\sum_{t=1}^{N} v_{rt}m_{tj}\right)\left(\sum_{w=1}^{N} v_{sw}m_{wj}\right) \\ &\quad C\mathrm{vec}^{-1}\left[G_{rs}\mathrm{vec}\left[B\Sigma_\eta B^{\mathrm{T}}\right]\right]C^{\mathrm{T}}.\end{aligned} \tag{36}$$

By applying the trace operator and summing for j that goes from 1 to N, we prove the claim. Note that this equation reduces to (18) for $M = I_N$. □

Proof of Remark 4. From equation (4), we can write the following relationship for the steady-state covariance matrix of the modal dynamics:

$$\begin{aligned}\widetilde{\Xi}_\infty^Q &= (V^{\mathrm{T}}RV\otimes F + \Lambda\otimes\Gamma)\widetilde{\Xi}_\infty^Q(V^{\mathrm{T}}RV\otimes F + \Lambda\otimes\Gamma)^{\mathrm{T}} \\ &\quad + (V^{\mathrm{T}}RQ\otimes B)(I_N\otimes\Sigma_\eta)(V^{\mathrm{T}}RQ\otimes B)^{\mathrm{T}}.\end{aligned} \tag{37}$$

Noting that

$$(V^{\mathrm{T}}RQ)_{rs} = \sum_{j=1}^{N}\left(\sum_{t=1}^{N} v_{rt}q_{tj}\right)\left(\sum_{w=1}^{N} v_{sw}q_{wj}\right), \tag{38}$$

we obtain the following expression for the N^2 blocks of size $n\times n$ of $\widetilde{\Xi}_\infty^Q$:

$$\begin{aligned}\left(\widetilde{\Xi}_\infty^Q\right)_{1s} &= \left(\widetilde{\Xi}_\infty^Q\right)_{s1} = 0, \qquad s = 1,\dots,N, \\ \left(\widetilde{\Xi}_\infty^Q\right)_{rs} &= (F-\lambda_r\Gamma)\left(\widetilde{\Xi}_\infty^Q\right)_{rs}(F-\lambda_s\Gamma)^{\mathrm{T}} \\ &\quad + \sum_{j=1}^{N}\left(\sum_{t=1}^{N} v_{rt}q_{tj}\right)\left(\sum_{w=1}^{N} v_{sw}q_{wj}\right)B\Sigma_\eta B^{\mathrm{T}}, \\ &\qquad r,s = 2,\dots,N.\end{aligned} \tag{39}$$

Transforming back to the original coordinates yields that the i-th diagonal block of Ξ_∞^Q can be written as

$$\begin{aligned}\left(\Xi_\infty^Q\right)_{ii} &= \sum_{r=2}^{N} v_{ri} \sum_{s=2}^{N} v_{si} \left(\widetilde{\Xi}_\infty^Q\right)_{rs} \\ &= \sum_{r=2}^{N}\sum_{s=2}^{N} v_{ri}v_{si} \sum_{j=1}^{N} \left(\sum_{t=1}^{N} v_{rt}q_{tj}\right)\left(\sum_{w=1}^{N} v_{sw}q_{wj}\right) \\ &\quad \mathrm{vec}^{-1}\left[G_{rs}\mathrm{vec}\left[B\Sigma_\eta B^{\mathrm{T}}\right]\right],\end{aligned} \tag{40}$$

for all $i = 1, \ldots, N$. Combining (40) with (25) yields

$$\begin{aligned}(R\otimes I_p)\Sigma_\infty(R\otimes I_p)_{ii} = \sum_{r=2}^{N}\sum_{s=2}^{N}\Bigg[v_{ri}v_{si}\sum_{j=1}^{N}\left(\sum_{t=1}^{N} v_{rt}q_{tj}\right) \\ \left(\sum_{w=1}^{N} v_{sw}q_{wj}\right) C\mathrm{vec}^{-1}\left[G_{rs}\mathrm{vec}\left[B\Sigma_\eta B^{\mathrm{T}}\right]\right]C^{\mathrm{T}}\Bigg].\end{aligned} \tag{41}$$

By recalling the hypothesis that $M = Q$, applying the trace operator, and using Proposition 4, for all $i = 1, \ldots, N$, we determine that,

$$\mathrm{Tr}\left((R\otimes I_p)\Sigma_\infty^Q(R\otimes I_p)\right)_{ii} = \mathrm{Vul}(i, M). \tag{42}$$

□

Proof of Remark 5. Since Q and L commute, they share the same eigenvectors, which are collated in matrix V. Obviously, for Q to commute with a symmetric matrix, it must also be symmetric. We identify as θ_1 the eigenvalue of Q associated with $\mathbb{1}_N$ (first column of V), and we order the remaining (real) eigenvalues $\theta_2, \ldots, \theta_N$ in ascending order. Given that R is a projector from $\mathbb{R}^N$ to $\mathbb{1}_N^\perp$, we have

1) $V^{\mathrm{T}}RQ = \Theta V^{\mathrm{T}}$
2) $V^{\mathrm{T}}RQQ^{\mathrm{T}}RV \otimes B\Sigma_\eta B^{\mathrm{T}} = \Theta^2 \otimes B\Sigma_\eta B^{\mathrm{T}}$

We utilize these considerations in the recursion for $\widetilde{\Xi}_k^Q$, which follows from (4):

$$\begin{aligned}\widetilde{\Xi}_{k+1}^Q = (V^{\mathrm{T}}RV\otimes F + \Lambda\otimes\Gamma)\widetilde{\Xi}_k^Q(V^{\mathrm{T}}RV\otimes F + \Lambda\otimes\Gamma)^{\mathrm{T}} \\ + (V^{\mathrm{T}}RQQ^{\mathrm{T}}RV)\otimes B\Sigma_\eta B^{\mathrm{T}}.\end{aligned} \tag{43}$$

From equation (43), the N^2 blocks of size $n \times n$ of $\widetilde{\Xi}_\infty^Q$ can be written as

$$\left(\widetilde{\Xi}_\infty^Q\right)_{rs} = \left(\widetilde{\Xi}_\infty^Q\right)_{sr} = 0, \qquad r = 1 \vee r \neq s, \tag{44a}$$

$$\begin{aligned}\left(\widetilde{\Xi}_\infty^Q\right)_{rr} = (F - \lambda_r\Gamma)\left(\widetilde{\Xi}_\infty^Q\right)_{rr}(F - \lambda_r\Gamma)^{\mathrm{T}} + \theta_r^2 B\Sigma_\eta B^{\mathrm{T}}, \\ r = 2, \ldots, N.\end{aligned} \tag{44b}$$

Applying the vectorization operator to (44b) yields

$$\mathrm{vec}\left[\left(\widetilde{\Xi}_\infty^Q\right)_{rr}\right] = \theta_r^2 G_{rr}\mathrm{vec}\left[B\Sigma_\eta B^{\mathrm{T}}\right]. \tag{45}$$

Transforming back to the original coordinates,

$$\begin{aligned}\left(\Xi_\infty^Q\right)_{ij} &= \sum_{r=2}^{N} v_{ri}\sum_{s=2}^{N} v_{sj}\left(\widetilde{\Xi}_\infty^Q\right)_{rs} \\ &= \sum_{r=2}^{N}\theta_r^2 v_{ri}v_{rj}\mathrm{vec}^{-1}\left[G_{rr}\mathrm{vec}\left[B\Sigma_\eta B^{\mathrm{T}}\right]\right].\end{aligned} \tag{46}$$

Finally, by using equation (24), we get

$$\begin{aligned}&\mathrm{Tr}\left((R\otimes I_p)\Sigma_\infty^Q(R\otimes I_p)\right)_{ii} \\ &= \sum_{r=2}^{N}\theta_r^2 v_{ri}^2\,\mathrm{Tr}\left(C\mathrm{vec}^{-1}\left[G_{rr}\mathrm{vec}\left[B\Sigma_\eta B^{\mathrm{T}}\right]\right]C^{\mathrm{T}}\right),\end{aligned} \tag{47}$$

from which the claim follows. □

ACKNOWLEDGEMENT

P. De Lellis was supported by the program "STAR 2018" of the University of Naples Federico II and Compagnia di San Paolo, Istituto Banco di Napoli - Fondazione, project ACROSS. M. Porfiri was supported by the National Science Foundation under grant number CMMI 1561134 and the program of the region of Murcia (Spain), "Call for Fellowships for Guest Researcher Stays at Universities and OPIS," project 21144/IV/19. Both the authors would like to express their gratitude to Dr. M. Ruiz Marín for useful discussion.

REFERENCES

[1] R. Kumar, J. Novak, and A. Tomkins, "Structure and evolution of online social networks," in *Link Mining: Models, Algorithms, and Applications*. Springer, 2010, pp. 337–357.
[2] T. Vicsek and A. Zafeiris, "Collective motion," *Physics Reports*, vol. 517, no. 3-4, pp. 71–140, 2012.
[3] G. A. Pagani and M. Aiello, "The Power Grid as a complex network: A survey," *Physica A*, vol. 392, no. 11, pp. 2688–2700, 2013.
[4] E. Bullmore and O. Sporns, "Complex brain networks: graph theoretical analysis of structural and functional systems," *Nature Reviews Neuroscience*, vol. 10, no. 3, pp. 186–198, 2009.
[5] J. Runge, S. Bathiany, E. Bollt, G. Camps-Valls, D. Coumou, E. Deyle, C. Glymur, M. Kretschmer, M. D. Mahecha, J. Munoz-Mari, E. H. van Nes, J. Peters, R. Quax, M. Reichstein, M. Scheffer, B. Schölkopf, P. Spirtes, G. Sugihara, J. Sun, K. Zhang, and J. Zscheischler, "Inferring causation from time series in earth system sciences," *Nature Communications*, vol. 10, no. 2553, pp. 1–13, 2019.
[6] Y. Yang, T. Nishikawa, and A. E. Motter, "Small vulnerable sets determine large network cascades in power grids," *Science*, vol. 358, no. 6365, p. eaan3184, 2017.
[7] Y. Berezin, A. Bashan, M. M. Danziger, D. Li, and S. Havlin, "Localized attacks on spatially embedded networks with dependencies," *Scientific Reports*, vol. 5, p. 8934, 2015.
[8] Y. Tang, F. Qian, H. Gao, and J. Kurths, "Synchronization in complex networks and its application–a survey of recent advances and challenges," *Annual Reviews in Control*, vol. 38, no. 2, pp. 184–198, 2014.
[9] P. Hines, K. Balasubramaniam, and E. C. Sanchez, "Cascading failures in power grids," *IEEE Potentials*, vol. 28, no. 5, pp. 24–30, 2009.
[10] Y.-Y. Liu and A.-L. Barabási, "Control principles of complex systems," *Reviews of Modern Physics*, vol. 88, no. 3, p. 035006, 2016.
[11] A. Strandburg-Peshkin, D. Papageorgiou, M. C. Crofoot, and D. R. Farine, "Inferring influence and leadership in moving animal groups," *Philosophical Transactions of the Royal Society B: Biological Sciences*, vol. 373, no. 1746, p. 20170006, 2018.
[12] J. T. Lizier and M. Prokopenko, "Differentiating information transfer and causal effect," *The European Physical Journal B*, vol. 73, pp. 605—615, 2010.
[13] M. Tyloo, L. Pagnier, and P. Jacquod, "The key player problem in complex oscillator networks and electric power grids: Resistance centralities identify local vulnerabilities," *Science Advances*, vol. 5, no. 11,eaaw8359, pp. 1–9, 2019.
[14] L. V. Gambuzza, A. Buscarino, L. Fortuna, M. Porfiri, and M. Frasca, "Analysis of dynamical robustness to noise in power grids," *IEEE Journal on Emerging and Selected Topics in Circuits and Systems*, vol. 7, no. 3, pp. 413–421, 2017.
[15] L. Pagnier and P. Jacquod, "Optimal placement of inertia and primary control: a matrix perturbation theory approach," *IEEE Access*, vol. 7, pp. 145 889–145 900, 2019.
[16] A. Buscarino, L. V. Gambuzza, M. Porfiri, L. Fortuna, and M. Frasca, "Robustness to noise in synchronization of complex networks," *Scientific Reports*, vol. 3, no. 1, pp. 1–6, 2013.

[17] M. Porfiri and M. Frasca, "Robustness of synchronization to additive noise: how vulnerability depends on dynamics," *IEEE Transactions on Control of Network Systems*, vol. 6, no. 1, pp. 375–387, 2018.

[18] K. Fitch and N. E. Leonard, "Joint centrality distinguishes optimal leaders in noisy networks," *IEEE Transactions on Control of Network Systems*, vol. 3, no. 4, pp. 366–378, 2015.

[19] S. Patterson, Y. Yi, and Z. Zhang, "A resistance-distance-based approach for optimal leader selection in noisy consensus networks," *IEEE Transactions on Control of Network Systems*, vol. 6, no. 1, pp. 191–201, 2018.

[20] E. Mackin and S. Patterson, "Optimizing the coherence of a network of networks," *IEEE Transactions on Control of Network Systems*, 2020.

[21] A. Salavaty, M. Ramialison, and P. D. Currie, "Integrated value of influence: An integrative method for the identification of the most influential nodes within networks," *Patterns*, p. 100052, 2020.

[22] H. H. Weerts, P. M. Van den Hof, and A. G. Dankers, "Prediction error identification of linear dynamic networks with rank-reduced noise," *Automatica*, vol. 98, pp. 256–268, 2018.

[23] J. Gonçalves and S. Warnick, "Necessary and sufficient conditions for dynamical structure reconstruction of lti networks," *IEEE Transactions on Automatic Control*, vol. 53, no. 7, pp. 1670–1674, 2008.

[24] Y. Yuan, G.-B. Stan, S. Warnick, and J. Goncalves, "Robust dynamical network structure reconstruction," *Automatica*, vol. 47, no. 6, pp. 1230–1235, 2011.

[25] D. Materassi and G. Innocenti, "Topological identification in networks of dynamical systems," *IEEE Transactions on Automatic Control*, vol. 55, no. 8, pp. 1860–1871, 2010.

[26] F. Sepehr and D. Materassi, "Blind learning of tree network topologies in the presence of hidden nodes," *IEEE Transactions on Automatic Control*, vol. 65, no. 3, pp. 1014–1028, 2019.

[27] S. Talukdar, D. Deka, H. Doddi, D. Materassi, M. Chertkov, and M. V. Salapaka, "Physics informed topology learning in networks of linear dynamical systems," *Automatica*, vol. 112, p. 108705, 2020.

[28] D. Hayden, Y. Yuan, and J. Gonçalves, "Network identifiability from intrinsic noise," *IEEE Transactions on Automatic Control*, vol. 62, no. 8, pp. 3717–3728, 2016.

[29] Z. Yue, J. Thunberg, W. Pan, L. Ljung, and J. Gonçalves, "Linear dynamic network reconstruction from heterogeneous datasets," *IFAC-PapersOnLine*, vol. 50, no. 1, pp. 10 586–10 591, 2017.

[30] E. Betti, "Teoria della elasticità," *Il Nuovo Cimento (1869-1876)*, vol. 7, no. 1, pp. 158–180, 1872.

[31] J. Rayleigh, *Treatise on Sound vol II*. London: Macmillan, 1878.

[32] C. Godsil and G. F. Royle, *Algebraic graph theory*. Springer Science & Business Media, 2013, vol. 207.

[33] R. A. Horn and C. R. Johnson, *Topics in matrix analysis*. Cambridge University Press, 1994.

[34] R. Olfati-Saber and R. M. Murray, "Consensus problems in networks of agents with switching topology and time-delays," *IEEE Transactions on Automatic Control*, vol. 49, no. 9, pp. 1520–1533, 2004.

[35] O. L. V. Costa, M. D. Fragoso, and R. P. Marques, *Discrete-time Markov jump linear systems*. Springer Science & Business Media, 2006.

[36] B. Klinger and N. Blüthgen, "Reverse engineering gene regulatory networks by modular response analysis–a benchmark," *Essays in Biochemistry*, vol. 62, no. 4, pp. 535–547, 2018.

[37] R. W. Newcomb, *Linear multiport synthesis*. McGraw-Hill, 1966.

[38] M. Pirani and S. Sundaram, "Spectral properties of the grounded Laplacian matrix with applications to consensus in the presence of stubborn agents," in *2014 American Control Conference*. IEEE, 2014, pp. 2160–2165.

[39] Y. Chen, J. Lu, X. Yu, and Z. Lin, "Consensus of discrete-time second-order multiagent systems based on infinite products of general stochastic matrices," *SIAM Journal on Control and Optimization*, vol. 51, no. 4, pp. 3274–3301, 2013.

[40] M. Porfiri, R. R. Sattanapalle, S. Nakayama, J. Macinko, and R. Sipahi, "Media coverage and firearm acquisition in the aftermath of a mass shooting," *Nature Human Behaviour*, vol. 3, no. 9, pp. 913–921, 2019.

[41] M. Porfiri, R. Barak-Ventura, and M. R. Marín, "Self-protection versus fear of stricter firearm regulations: Examining the drivers of firearm acquisitions in the aftermath of a mass shooting," *Patterns*, vol. 1, no. 6, p. 100082, 2020.

[42] S. A. Pettersen, D. Johansen, H. Johansen, V. Berg-Johansen, V. R. Gaddam, A. Mortensen, R. Langseth, C. Griwodz, H. K. Stensland, and P. Halvorsen, "Soccer video and player position dataset," in *Proceedings of the 5th ACM Multimedia Systems Conference*, 2014, pp. 18–23.

[43] S. Butail and M. Porfiri, "Detecting switching leadership in collective motion," *Chaos: An Interdisciplinary Journal of Nonlinear Science*, vol. 29, no. 1, p. 011102, 2019.

[44] L. Bornn, D. Cervone, and J. Fernandez, "Soccer analytics: Unravelling the complexity of "the beautiful game"," *Significance*, vol. 15, no. 3, pp. 26–29, 2018.

[45] J. Clerk Maxwell, "L. on the calculation of the equilibrium and stiffness of frames," *The London, Edinburgh, and Dublin Philosophical Magazine and Journal of Science*, vol. 27, no. 182, pp. 294–299, 1864.

[46] H. A. Lorentz, "The theorem of Poynting concerning the energy in the electromagnetic field and two general propositions concerning the propagation of light," *Amsterdammer Akademie der Wetenschappen*, vol. 4, p. 176, 1896.

Pietro De Lellis (M'14) was born in Naples, Italy, in 1983. He received the Ph.D. degree in automation engineering from the University of Naples Federico II, Naples, Italy, in 2009. He spent six months at New York University Tandon School of Engineering, Brooklyn, USA as a visiting Ph.D. student from January to July 2009. On April 2010, he was appointed Visiting Professor at the Department of Mechanical and Aerospace Engineering of New York University Tandon School of Engineering, where he taught the course on automatic control. From 2010 to 2014, he was Adjunct Professor with Accademia Aeronautica (the Italian equivalent of the Air Force Institute of Technology), Pozzuoli, Italy. During the summer periods, from 2012 to 2014, he was a Postdoctoral Fellow at New York University Tandon School of Engineering, and worked on the projects "Collaborative research: Geometry of group behaviors with application to fish schooling" and "CAREER: Guidance and control of fish shoals using bio-mimetic robots." In 2014, he obtained the National Habilitation as Associate Professor. He is currently a Tenured Assistant Professor of Automatic Control with the University of Naples Federico II since 2014. He has authored more than 60 scientific publications that, according to Google Scholar (June 2020), received over 1700 citations. His research interests include analysis, synchronization, and control of complex networks, collective behavior analysis, formation control, decentralized estimation, and evolving financial networks. Dr. De Lellis serves on the editorial board of several international scientific journals and conferences.

Maurizio Porfiri (SM'12, F'19) received M.Sc. and Ph.D. degrees in Engineering Mechanics from Virginia Tech, in 2000 and 2006; a "Laurea" in Electrical Engineering (with honours) and a Ph.D. in Theoretical and Applied Mechanics from "Sapienza" University of Rome and the University of Toulon (dual degree program between Italy and France), in 2001 and 2005, respectively. He is currently an Institute Professor at New York University Tandon School of Engineering, Brooklyn, USA, with appointments in the Departments of Mechanical and Aerospace Engineering, Biomedical Engineering, and Civil and Urban Engineering. Dr. Porfiri is a Fellow of the American Society of Mechanical Engineers (ASME) and the Institute of Electrical and Electronic Engineers (IEEE). He has served in the Editorial Board of ASME Journal of Dynamics Systems, Measurements and Control, ASME Journal of Vibrations and Acoustics, IEEE Control Systems Letters, IEEE Transactions on Circuits and Systems I, and Mechatronics. Dr. Porfiri is the Director of the Dynamical Systems Laboratory and he is engaged in conducting and supervising research on dynamical systems theory, multiphysics modeling, and underwater robotics. He is the author of more than 300 journal publications and the recipient of the National Science Foundation CAREER award. He has been included in the "Brilliant 10" list of Popular Science in 2010 and his research featured in all the major media outlets, including CNN, NPR, Scientific American, and Discovery Channel. Other significant recognitions include invitations to the Frontiers of Engineering Symposium and the Japan-America Frontiers of Engineering Symposium organized by National Academy of Engineering; the Outstanding Young Alumnus award by the college of Engineering of Virginia Tech; the ASME Gary Anderson Early Achievement Award; the ASME DSCD Young Investigator Award; and the ASME C.D. Mote, Jr. Early Career Award.